Electronic Supplementary Material (ESI) for Journal of Materials Chemistry C.

Electronic Supplementary Information

Inhibition of buried cavities and defects in metal halide perovskite photodetectors *via* two-step spin-coating method

Silei Wang[1], Tengteng Li[1], Qingyan Li[1], Hongliang Zhao[1], Chenglong Zheng[1], Mengyao Li[1], Jitao Li[1], Yating Zhang[1]*, Jianquan Yao[1]*

[1] *Key Laboratory of Opto-Electronics Information Technology, Ministry of Education, School of Precision Instruments and Opto-Electronics Engineering, Tianjin University, Tianjin 300072, China*.

*Corresponding authors' e-mail: yating@tju.edu.cn, jqyao@ tju.edu.cn.

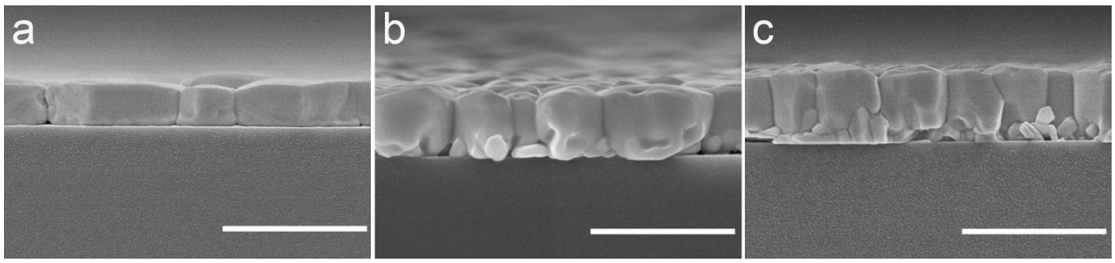

Figure S1. The cross-Section scanning electron microscope (SEM) images of perovskite prepared by (a)1 M, (b)1.3 M and (c)1.5 M PbI_2 react with 50 mg ml^{-1} via the two-step spin-coating method. The scale bar is 1μm.

Note: With the increase of PbI_2 precursor concentration, the thickness of perovskite film gradually increases. As shown in Figure S1, the grains span the perovskite film (~310 nm thickness) prepared by the 1 M PbI_2 precursor. However, the nanocavities and small spherical grains appear at the bottom interface of the perovskite film (~430 nm thickness) prepared by the 1.3 M PbI_2 precursor, and the perovskite film (~510 nm thickness) in Figure S1c is even worse.

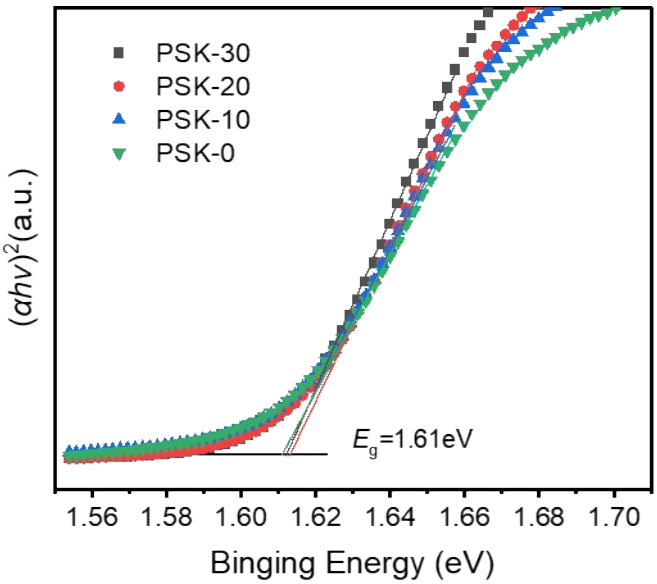

Figure S2. The band gap of perovskite film was calculated by Tauc Plot method

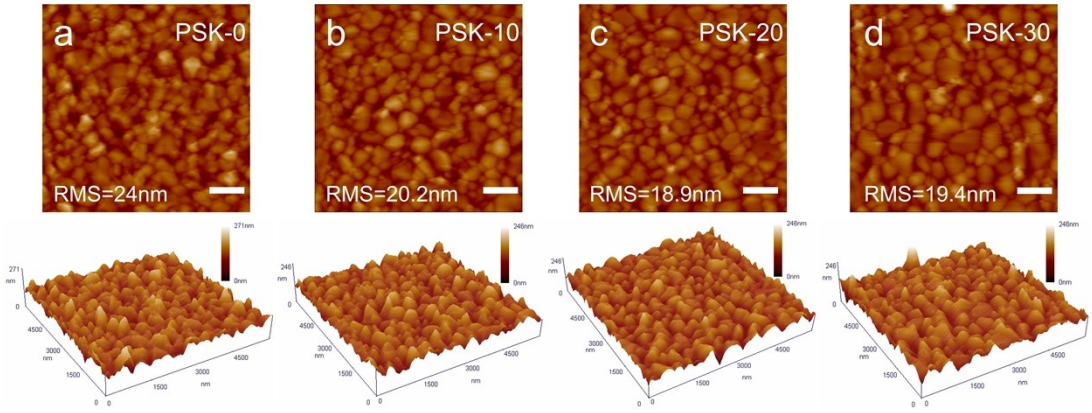

Figure S3. The atomic force microscope (top row) and 3D topography (bottom row) of the PSK-*x* (*x*=0, 10, 20 and 30), respectively. The root mean square (RMS) in the inset is the effective value of surface roughness. The scale bar is 1μm. The RMS value of surface roughness for PSK-*x* (*x*=0, 10, 20 and 30) varies from 24 to 19.4 nm with the increase of MAI introduction.

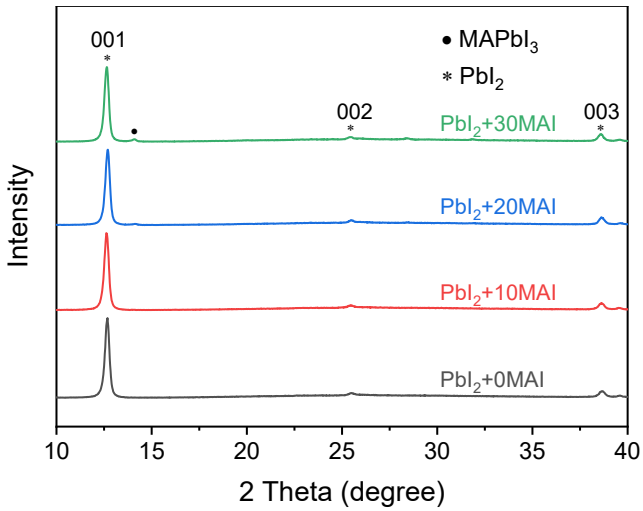

Figure S4. The XRD patterns of the PbI_2+xMAI (x=0, 10, 20 and 30), respectively. The weak $MAPbI_3$ peak can be observed on the substrate surface after the introduction of MAI.

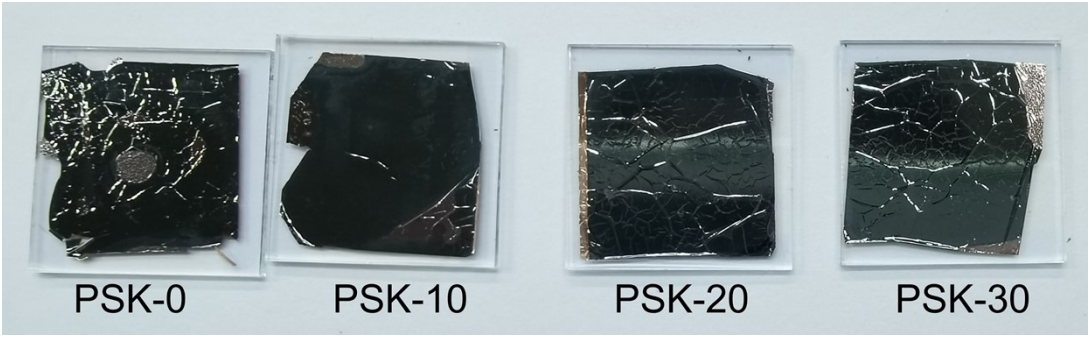

Figure S5. Optical image of PSK-*x* (*x*=0, 10, 20, 30) film after the lift-off process, respectively.

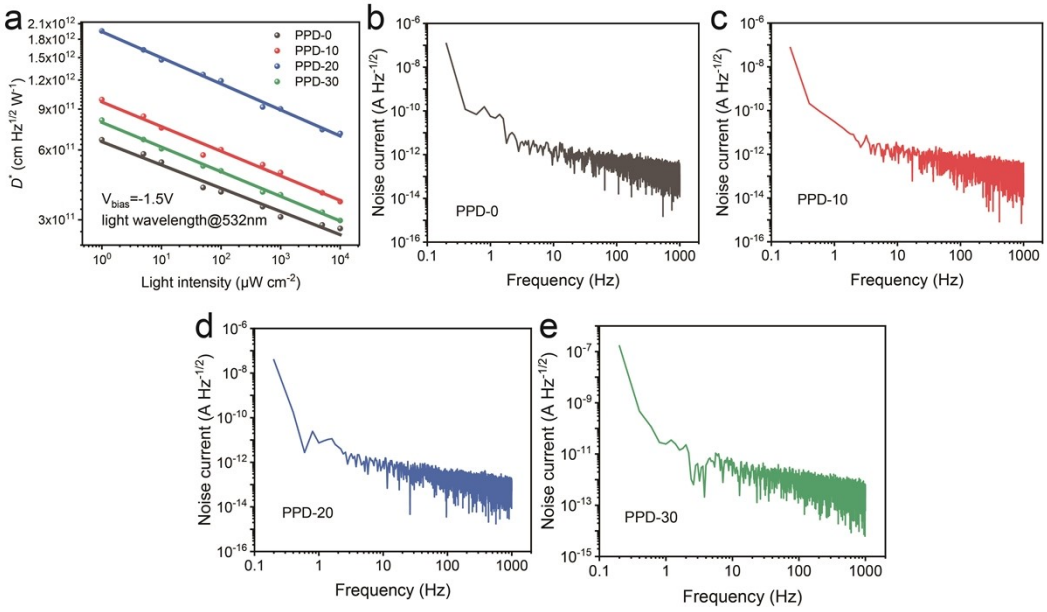

Figure S6. (a) The D^* of all PPDs calculated based on equation (4) under an applied voltage of −1.5 V. The i_n measured of is PPD-0, PPD-10, PPD-20 and PPD-30 are shown in Figures (b), (c), (d) and (e), respectively.

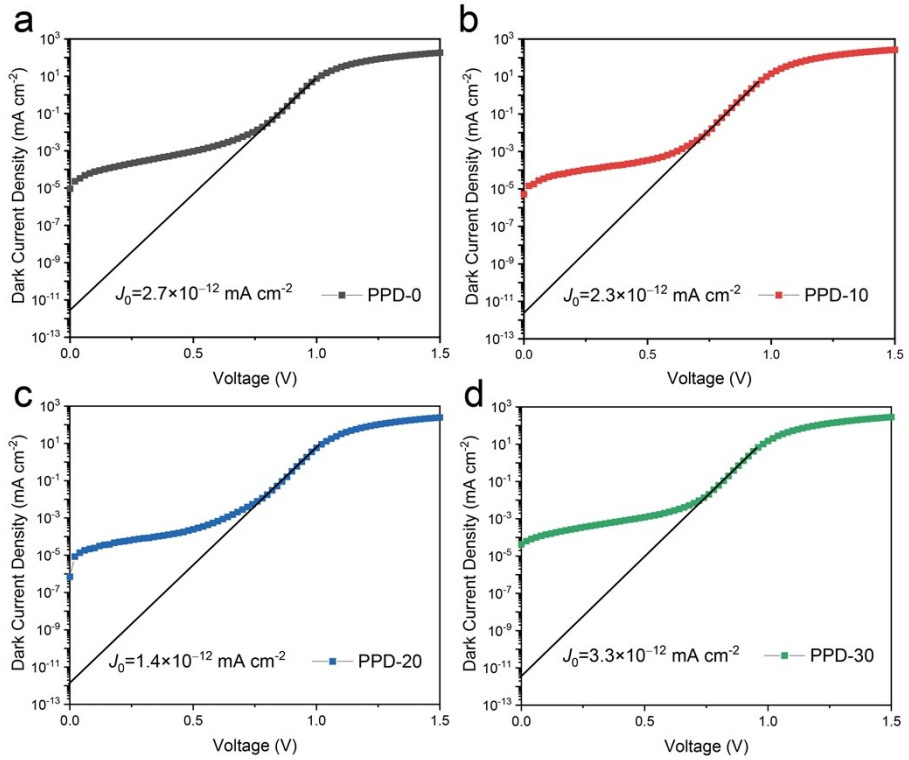

Figure S7. Semi-log plots of dark current densities versus voltage and the linear fitting for reverse saturation extraction. (a) PPD-0, (b) PPD-10, (c) PPD-20 and (d) PPD-30.

Table S1. Summary of performances of PPDs.

Device structure	R (bias, light source & intensity)	Detectivity (D^*, Jones)	Response time (T_{rise}/T_{fall})	LDR (dB)	Ref.
ITO/PEPDOT:PSS/ $FA_{0.85}Cs_{0.15}Sn_{0.5}Pb_{0.5}I_3$ /$PC_{61}BM$/ZrAcac/Ag	0.53 A W^{-1} (940 nm)	6×10^{12} (940 nm)	0.86 μs.	103	1
ITO/NiO_x:PbI_2/$MAPbI_3$/C60/ BCP/Ag.	0.5 A W^{-1} (~750 nm)	6×10^{12}	168 ns	112	2
ITO/SnO_2/ $(FAPbI_3)_{0.97}(MAPbBr_3)_{0.03}$ /Spiro-MeoTAD/Au	—	1.2×10^{12}	3/6 μs (−0.5 V)	80	3
ITO/SnO_x/$PC_{61}BM$/$Cs_{0.18}FA_{0.82}Pb(I_{0.82}Br_{0.18})_3$/PTAA/MoCr	0.36 A W^{-1} (−0.5 V, 680 nm)	2.1×10^{13} (−0.5 V, 680 nm)	2.7/2.3 μs	—	4
ITO/PTAA/ $MAPbI_3$/IEICO/C_{60}/BCP/Cu	0.28 A W^{-1} (0 V, 650 nm)	1.45×10^{12} (650 nm)	27 ns	198	5
ITO/PTAA/MAPbI3/F8IC:PTB7-Th/ C_{60}/ BCP/ Cu	0.43 A W^{-1} (0 V, 710 nm)	2.3×10^{11} (0 V, 870 nm)	35/20 μs	191	6
ITO/PEDOT:PSS/$MAPbI_{3-x}Cl_x$/$PC_{61}BM$/PFN/Al	—	4×10^{14} (0 V, 550 nm)	180/160 ns	100	7
FTO/CdS/$MAPbI_3$/Spiro-OMeTAD/Ag	0.48 A W^{-1} (0 V, 700nm)	2.1×10^{13} (0 V, 700 nm)	0.54/2.21 ms	—	8
FTO/$SrTiO_3$/$MAPbI_3$/ Spiro-OMeTAD/Ag	0.73 A W^{-1} (0 V, 550 nm)	—	100 ms	—	9
ITO/OTPD/$MAPbI_3$/PCBM/C_{60}/Al	0.21 A W^{-1} (−0.1 V, white light)	7.4×10^{12} (−0.1 V, 680 nm,)	120 ns	94	10
ITO/$MAPbI_3$/TPD-Si_2/MoO_3/Ag	242 A W^{-1} (−1 V, 740 nm)	—	10 μs	85	11
ITO/PTAA/$MAPbI_3$/C_{60}/BCP/Cu	0.47 A W^{-1} (0 V, 680 nm)	7.8×10^{12} (0 V, 700 nm)	0.95 ns	—	12
ITO/PTAA/$MAPbI_3$/PDPPTDTPT:PCBM/BCP/Cu	—	10^{11} (−0.2 V, 900 nm)	5ns	95	13
TETA-GR/MoS_2/$MAPbI_3$/PTAA/Au	0.42 A W^{-1} (0 V, ~750 nm)	1.1×10^{10} (0 V, 532 nm)	1.63/0.98 μs	112	14
co-GR/MoS_2/$MAPbI_3$/PCBM/BCP/Al	0.41A W^{-1} (0 V, 700 nm, 407 μW cm^{-2})	8×10^{10} (0 V, 700 nm, 407 μW cm^{-2})	800/500 ms	117	15
TFSA-GR/PEDOT:GQDs/$MAPbI_3$:GQDs/PCBM/BCP/Al	0.44 A W^{-1} (0 V, ~700 nm)	8.7×10^{12} (0 V, ~700 nm)	0.56/0.96 μs	100	16
ITO/PET/PDMS/ITO/PET/$MAPbI_3$/ Au	0.418 A W^{-1} (1 V, white light, 10 μW cm^{-2})	1.2×10^{13}	80/80 ms	—	17
ITO/PEDOT:PSS/$MAPbI_3$/$PC_{61}BM$/C_{60}/LiF/Ag	—	3.0×10^{12} (1 V, 700 nm)	1.7/1 μs	170	18
ITO/PEDOT:PSS/MAPbI3/PC61BM/BCP/Au (PPD-0, PPD-10, PPD-20, PPD-30)	0.5 A W^{-1} 0.66 A W^{-1} 0.79 A W^{-1} 0.74 A W^{-1} (−1.5 V, 532 nm, 1 μW cm^{-2})	6.6×10^{11} 9.9×10^{11} 1.95×10^{12} 8.1×10^{11} (−1.5 V, 532 nm, 1 μW cm^{-2})	3.1/74.5 μs 2.8/73.6 μs 2.6/72.8 μs 2.3/76.7 μs	86 100 106 86	This work

References

1. H. Liu, H. L. Zhu, Z. Wang, X. Wu, Z. Huang, M. R. Huqe, J. A. Zapien, X. Lu and W. C. H. Choy, *Advanced Functional Materials*, 2021, **31**, 2010532.
2. H. L. Zhu, J. Cheng, D. Zhang, C. Liang, C. J. Reckmeier, H. Huang, A. L. Rogach and W. C. Choy, *ACS Nano*, 2016, **10**, 6808-6815.
3. Y. Wang, X. Zhang, Q. Jiang, H. Liu, D. Wang, J. Meng, J. You and Z. Yin, *ACS Applied Materials & Interfaces*, 2018, **10**, 6505-6512.
4. A. J. J. M. van Breemen, R. Ollearo, S. Shanmugam, B. Peeters, L. C. J. M. Peters, R. L. van de Ketterij, I. Katsouras, H. B. Akkerman, C. H. Frijters, F. Di Giacomo, S. Veenstra,

R. Andriessen, R. A. J. Janssen, E. A. Meulenkamp and G. H. Gelinck, *Nature Electronics*, 2021, **4**, 818-826.
5. C. Li, J. Lu, Y. Zhao, L. Sun, G. Wang, Y. Ma, S. Zhang, J. Zhou, L. Shen and W. Huang, *Small*, 2019, **15**, 1903599.
6. C. Li, H. Wang, F. Wang, T. Li, M. Xu, H. Wang, Z. Wang, X. Zhan, W. Hu and L. Shen, *Light Sci Appl*, 2020, **9**, 31.
7. L. Dou, Y. M. Yang, J. You, Z. Hong, W. H. Chang, G. Li and Y. Yang, *Nat Commun*, 2014, **5**, 5404.
8. F. Cao, L. Meng, M. Wang, W. Tian and L. Li, *Adv Mater*, 2019, **31**, 1806725.
9. F. Cao, W. Tian, M. Wang and L. Li, *ACS Photonics*, 2018, **5**, 3731-3738.
10. Y. Fang and J. Huang, *Adv Mater*, 2015, **27**, 2804-2810.
11. R. Dong, Y. Fang, J. Chae, J. Dai, Z. Xiao, Q. Dong, Y. Yuan, A. Centrone, X. C. Zeng and J. Huang, *Adv Mater*, 2015, **27**, 1912-1918.
12. L. Shen, Y. Fang, D. Wang, Y. Bai, Y. Deng, M. Wang, Y. Lu and J. Huang, *Adv Mater*, 2016, **28**, 10794-10800.
13. L. Shen, Y. Lin, C. Bao, Y. Bai, Y. Deng, M. Wang, T. Li, Y. Lu, A. Gruverman, W. Li and J. Huang, *Materials Horizons*, 2017, **4**, 242-248.
14. D. H. Shin, J. S. Ko, S. K. Kang and S.-H. Choi, *ACS Appl Mater Interfaces*, 2020, **12**, 4586-4593.
15. D. H. Shin, S. H. Shin and S.-H. Choi, *Applied Surface Science*, 2020, **514**.
16. D. H. Shin, S. H. Shin, S. G. Lee, S. Kim and S.-H. Choi, *ACS Sustainable Chemistry & Engineering*, 2019, **7**, 19961-19968.
17. S. F. Leung, K. T. Ho, P. K. Kung, V. K. S. Hsiao, H. N. Alshareef, Z. L. Wang and J. H. He, *Adv Mater*, 2018, **30**, 1704611.
18. Q. Lin, A. Armin, D. M. Lyons, P. L. Burn and P. Meredith, *Adv Mater*, 2015, **27**, 2060-2064.